JITH 2017
18èmes Journées Internationales de Thermique (JITH 2017)
Monastir (Tunisie), 25 - 27 Octobre 2017

Modeling and simulation of heat and mass transfer during biomass gasification in a packed bed downdraft reactor

Mohamed Ali MASMOUDI[a], Melik SAHRAOUI[b], Kamel HALOUANI[a]
[a] Micro Electro Thermal Systems (UR13ES76), ENIS-IPEIS, University of Sfax, Road Menzel Chaker Km 0.5 B.P: 1172, 3018 Sfax, Tunisia
[b] Applied Mechanics and Systems Research Laboratory, Polytechnic Engineering School of Tunis, University of Carthage, La Marsa-Tunis, Tunisia
mmedali1@yahoo.fr; m_sahraoui@yahoo.com; ***kamel.halouani@ipeis.rnu.tn***

Abstract: A two dimensional numerical modeling of transfer phenomena in a pilot downdraft gasifier is developed based on the principles of conservation of mass, energy and momentum coupled with the different thermo-chemical reactions involved in the different steps of the process (namely pyrolysis, partial oxidation and reduction reactions). The packed bed reactor was considered as a porous medium and the set of conservation equations was written based on the local volume averaging approach. Validation of the developed model was carried out by comparing the numerical results with our own previous experimental data. The model is used to simulate the heat and mass transport fields in the computational domain and analyze the interaction between kinetic chemistry and transport phenomena.

Keywords: biomass, gasification, numerical modeling, heat and mass transfer, downdraft reactor, porous media

1. Introduction

Nowadays, the world energy demand growth due to the increase of energy intensive activities associated to modern life styles and the massive utilization of fossil fuels has led to several environmental problems which represent a threat to the human lives' on earth. Therefore, the exploring of renewable energy sources and eco-friendly technologies has become an urgent necessity. Biomass can be a potential and realistic alternative energy source that can partially substitute the fossil fuels. So far, it is expected that biomass energy, also termed as bioenergy, will satisfy 30% of the world energy demand [1]. The conversion of the different biomass resources into useful energy forms such as heat, electricity and biofuels in an efficient and clean way represents an attractive option for renewable energy production. Among the various conversion routes, gasification is a promising technology that enables the thermo-chemical conversion of biomass materials into a gas fuel. This gaseous fuel, commonly referred to as synthesis gas or syngas, consists of a mixture of carbon monoxide, hydrogen, traces of light hydrocarbons and other inert gases. It is a versatile energy carrier that can be used in both existing and novel energy conversion system like boilers, turbines, fuel cells and refineries.

Among the different reactors used for the gasification process, downdraft gasifier has been the subject of continuous research and development due to its relatively simple design, construction and operation [2]. Four sub-processes can be identified in a downdraft gasification unit. These are stratified from top to bottom as drying, pyrolysis, partial oxidation and reduction. Biomass is firstly heated up and dried at the top of the reactor. The second step of the conversion consists of the pyrolysis, which is a thermal decomposition of the solid biomass into a char and volatile compounds which undergo a partial oxidation step with the introduction of air from lateral nozzles. The air blown into the reactor partially oxidizes the charred particles and the different combustible gases produced during the pyrolysis step generating an intensive heat in both gas and solid (char) which partially shrinks. In the final reduction step, the heterogeneous reactions of the oxidation gases products (i.e. carbon dioxide and steam) take place over the char particles surfaces and yield the syngas at the outlet of the reactor. All these sub-processes are essentially governed by heat and mass transfer (i.e. heating rate and local temperature) in porous media.

Modeling of biomass gasification and combustion in packed bed reactors was performed in literature using different approaches [2-4]. These include the equilibrium modeling, the coupled kinetic and transport modeling and the artificial network modeling (ANN) [3, 4]. Exhaustive reviews with comparative studies of these various modeling approaches were presented in literature [3, 4]. Among these different modeling methods,

the coupled kinetic and transport models are among the most comprehensive and reliable models performed in literature [5]. They are based on conservation equations and kinetic parameters obtained from experiments. Therefore, they allow for of a better simulation of the process based on a precise description of the interaction between the chemical kinetics and the transport phenomena.

In this study, a coupled kinetic and transport numerical model is developed for biomass gasification in a pilot downdraft gasifier. The model comprises the main reacting zones of the gasifier. In addition, it considers the different relevant physical and chemical phenomena which take place during the conversion. These include the hydrodynamics of the gas flow through the porous packed bed, the heat transfer in the solid and gas phases as well as the interfacial convective flux between the two phases, the mass transfer of the gas species in the gas phase and the different homogeneous and heterogeneous chemical reactions. The developed model is used to simulate the heat and mass transport fields in the downdraft gasifier.

2. Model development

2.1. Physical model

The physical model is described by Figure 1. It consists of a packed bed of biomass particles which are undergoing the different thermo-chemical steps involved in the gasification process successively (pyrolysis, partial oxidation and gasification). The considered domain corresponds to a pilot scale downdraft gasifier designed by the authors and manufactured locally in Tunisia. The gasifier was described and experimented in a previous work [6]. The physical domain has a total length of 650 mm. Its radius is variable between 100 and 340 mm because of the specific conical geometry of the reactor. The air inlet nozzles are located at z=250 mm. A perforated grate is located at the bottom of the domain and is used to uphold the packed bed of biomass and char particles.

The porous media approach, known also as the quasi continuous, the macroscopic or the Euler- Euler approach [7-13], is selected for the model development. This approach is based on the continuous description of the solid phase and the gas phase forming the porous packed bed. Indeed, the different variables and properties are averaged over elementary volumes which contain both solid and gas phases. Consequently, the set of microscopic conservation equations valid at the point scale are transformed in a set of macroscopic conservation equations valid over the elementary volumes.

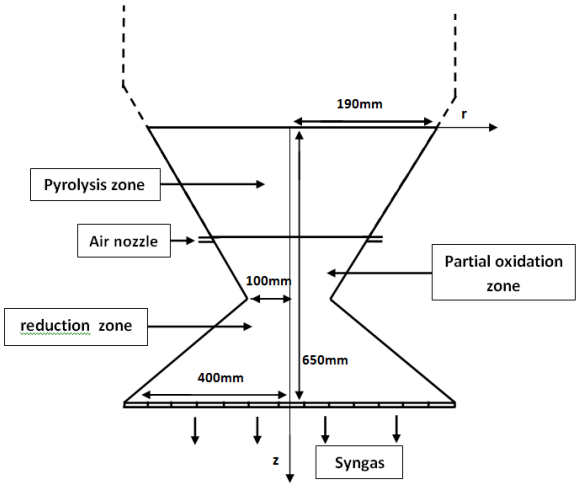

Figure 1. Physical model

2.2. Model assumption

The coupled transport and chemical phenomena occurring in the downdraft packed bed gasifier are implemented using the following simplification assumptions:

- The model is two dimensional and axi-symmetric.
- The biomass and char derived particles are assumed to have a spherical shape. The equivalent particle diameter is used in calculation.
- The diameter of biomass particles are assumed to remain constant during pyrolysis (i.e. shrinkage is negligible). The mass loss during pyrolysis is accounted for through a decrease in the biomass density. The biomass density decreases progressively as pyrolysis proceeds to reach the density of char which is calculated as:

$$\rho_{ch} = \nu_{C,f}\ \rho_b \quad (1)$$

Where $\nu_{C,f}$ is the final mass fraction of char after biomass pyrolysis is completed.

- The density of char particles is assumed to be constant. The char mass loss due to the heterogeneous oxidation reaction is accounted for through a decrease in the particle size.
- The biomass and char derived particles are assumed to be thermally thin during the conversion [13].
- Continuous and smooth shrinkage of the bed due to solid char consumption is assumed. In addition, the velocity is described here using the axial component while the radial component is neglected.
- Phenol is taken as representative model compound of the tar species.
- Water vapor and tar condensation in the reactor are neglected.
- The probable presence of turbulence at the vicinity of the air nozzles is implicitly accounted for through the correlations of the heat and mass transfer coefficients and the use of the eddy dissipation model for the homogeneous oxidation reactions [5].

2.3. Chemical mechanism

2.3.1. Pyrolysis reaction

2.3.1.1. Experimental procedure

The kinetic model used for the biomass pyrolysis reaction was determined experimentally. The thermal degradation of the biomass used in the experimental study on the downdraft gasifier (almond shell) [6] was carried out using a Thermo-Gravimetric apparatus (LabSys, SETARAM Corporation). A sample of about 25 mg of grinded almond shell was placed in a crucible and was subjected to a heating program from room temperature to 873K at a constant heating rate of 10K/min. A plateau at 423K was kept for 20 min to ensure the complete drying of the sample before its pyrolysis. The experiment was carried out in inert environment using argon as carrier gas with a flow rate of about 30 ml/min.

The mass loss and mass loss derivative (DTG) curves obtained are shown in Figure 2. The mass loss curve shows that the thermal decomposition of the material started at a temperature around 593K. The DTG curve indicates precisely the specific temperature interval for which thermal decomposition takes place and the temperatures for which high decomposition rates occur. Here, the curve shows that the largest fraction of the biomass material was degraded between 493K and 673K. One can notice the presence of a wide decomposition peak with low intensity preceded by a small shoulder. This shoulder is located at around 653K and is likely associated to the decomposition of the hemicellulose fraction of almond shell, while the main peak appears at approximately 693K and is associated to the decomposition of the cellulose fraction [14].

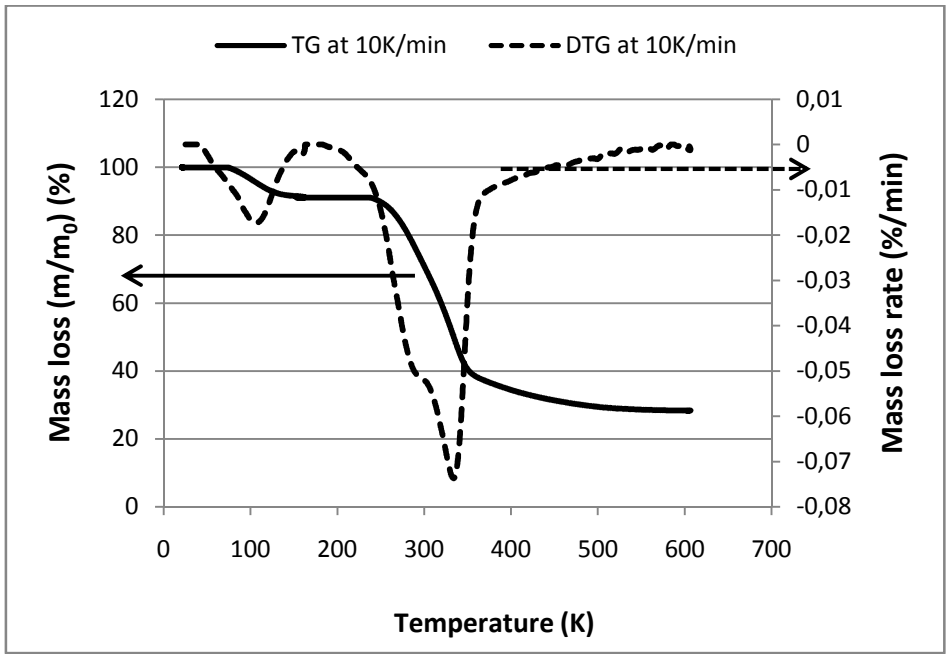

Figure 2. Mass loss (TG) curves Mass loss derivative (DTG) curves of almond shell at 10K/min

2.3.1.2. Kinetic model

The obtained DTG curve of almond shell pyrolysis experiment showed the presence of a main decomposition peak. This indicates that a one step global reaction scheme can be used to describe the kinetics of the almond shell pyrolysis reaction. The one step global reaction model is given by:

$$Almond\ shell \ \rightarrow \nu_C Char + \nu_V\ Volatiles \tag{2}$$

where ν_C and ν_V are the fractions of the char and volatiles products.
The kinetic of this reaction is described using an Arrhenius law equation and is given by:

$$k_p = A_p \exp\left(-\frac{E_p}{RT}\right) \tag{3}$$

Different methods were used in literature to determine the values of the kinetic parameters (activation energy E_p and pre-exponential factor A_p). These include the iso-conversional KAS model, the OFW model, the differential method and the Coats–Redfern method [15- 17]. Here, the differential method is used to determine the pyrolysis kinetic parameters. The obtained results for almond shell pyrolysis kinetic parameters are summarized in Table 1.

Table 1. Kinetic parameters of the almond shell pyrolysis reaction at 10°C/min

Activation energy E_a $(J.mol^{-1})$	*Pre-exponential factor* A (s^{-1})	*Determination coefficient* R^2
96 656. 27	$1.47\ 10^7$	0.9940

2.3.2. Partial oxidation reactions

The char and the volatile compounds generated in the pyrolysis step flow down in the reactor and penetrate into the partial oxidation zone where air is continuously supplied from lateral nozzles. The oxidation of the gaseous species is relatively fast. However, since oxygen is the limiting species, a two-step reaction model is used for the oxidation of the tar and the light gaseous species. The first step is a partial oxidation which yields carbon monoxide. In the second step, the carbon monoxide is oxidized to carbon dioxide. Moreover, the homogeneous oxidation reactions take place in the void spaces of the bed. Thus, the rate of gases oxidation is not only limited by the intrinsic kinetic but also by the mixing rate with oxygen from air. The oxidation rate is consequently expressed as the minimum of the kinetic and mixing rate [10, 18]:

$$r_j = min\left(r_{kin,j}, r_{mix,j}\right) \tag{4}$$

Where r_{kin} is chemical reaction rate and $r_{mix,j}$ is the mixing rate given by [10, 18]:

$$r_{mix,j} = 0.63\frac{\rho}{\bar{W}}\left(\frac{1.75(1-\varepsilon)V}{\varepsilon\, d_p}\right) min\left(\frac{y_i}{\nu_{i,j}}\right) \tag{5}$$

Where y_i and $\nu_{,j}$ are respectively the molar fraction and stoichiometric coefficient of the reactants involved in the homogeneous reaction *j*.
The kinetic data and rates of the considered homogeneous partial oxidation reactions are given in Table 2.
The oxidation of char particles occurs upon the introduction of air in the gasifier (eq. R9 in table 3). The products of this reaction include carbon monoxide and carbon dioxide. The proportion of each gas specie depends on the local temperature of the particles. The correlation describing the CO to CO_2 molar ratio as function of the char temperature is given by [19]:

$$\gamma(T_s) = \frac{n_{CO}}{n_{CO_2}} = 3 \cdot 10^8 exp\left(\frac{-30178}{T_s}\right) \tag{6}$$

On the other hand, the rate of the char oxidation could be governed by chemical kinetics or by mass transfer of oxygen to the particles surfaces. External mass transfer is generally the controlling mechanism because the intrinsic chemical rate of oxidation is very high. The effectiveness factor of this heterogeneous reaction was included in the kinetic rate in order to account for the internal mass transfer inside the char particles [13]. Thus, the overall rate of the char oxidation reaction considers both limiting phenomena (chemical and transport). The expression of the overall reaction rate is provided in Table 3.

2.3.3. Gasification reactions

The gasification reactions take place in last step of the conversion. The main reactions are the Water gas and Boudouard reaction given respectively by reactions (R10) and (R11) in Table 3. Contrarily to the char oxidation reaction, the gasification reactions are slow and dependent on the reactivity of the char [13]. The overall rate of the gasification reactions considers both chemical and physical phenomena and is set to be proportional to the difference between the reactants and products molar fractions scaled by the corresponding equilibrium constant [20]. The reduction reactions and their associated kinetic and overall rates are given in table 3.

Table 2. Homogeneous oxidation reactions considered in the model and their kinetic rates.

Reaction	Chemical reaction	Kinetic reaction rate (s^{-1})	Ref.
R1	$C_6H_6O + 4O_2 \rightarrow 6CO + 3H_2O$	$2.4 \times 10^{11} exp\left(-\frac{125520}{RT_g}\right)[C_6H_6O]^{-0.1}[O_2]^{1.85}$	[21]
R2	$CH_4 + 1.5O_2 \rightarrow CO + 2H_2O$	$5.012 \times 10^{11} exp\left(-\frac{200000}{RT_g}\right)[CH_4]^{0.5}[O_2]$	[22]
R3	$CO + 0.5O_2 \rightarrow CO_2$	$4.4 \times 10^{11} exp\left(-\frac{125520}{RT_g}\right)[CO]^{0.5}[O_2]^{1.25}$	[21]
R4	$H_2 + 0.5O_2 \rightarrow H_2O$	$10^{14} exp\left(-\frac{42000}{RT_g}\right)[H_2][O_2]$	[21]
R5	$C_6H_6 + 3O_2 \rightarrow 6CO + 3H_2$	$1.58 \times 10^{15} exp\left(-\frac{202600}{RT_g}\right)[C_6H_6][O_2]$	[22]
R6	$CH_4 + 0.5O_2 \rightarrow CO + 2H_2$	$4.996 \times 10^{13} exp\left(-\frac{202600}{RT_g}\right)[CH_4]^{0.7}[O_2]^{0.8}$	[22]
R7	$CH_4 + H_2O \rightarrow CO + 3H_2$	$3015\ exp\left(-\frac{125520}{RT_g}\right)\left([CH_4][H_2O] - \frac{[H_2]^3[CO]}{K_{1,eq}}\right)$	[23]
R8	$CO + H_2O \leftrightarrow CO_2 + H_2$	$2.78\ exp\left(-\frac{12600}{RT_g}\right)\left([H_2O][CO] - \frac{[H_2][CO_2]}{K_{2,eq}}\right)$	[23]

Table 3. Heterogeneous oxidation and reduction reactions considered in the model and their and chemical rates.

Reaction number	Reaction	Chemical rate (s^{-1})	Ref.
R9	$CH_{0.65}O_{0.25} + \left(\frac{2+\gamma}{1+\gamma} + 0.075\right)O_2 \rightarrow \left(\frac{\gamma}{1+\gamma}\right)CO + \left(\frac{1}{1+\gamma}\right)CO_2 + 0.325H_2O$	$\frac{[O_2]}{\frac{1}{h_m} + \frac{1}{CRF \cdot 4000exp\left(-\frac{80000}{RT_s}\right)}} A_p$	[8, 11]
R10	$CH_{0.65}O_{0.25} + 0.75\ H_2O \rightarrow CO + 1.075\ H_2$	$\frac{1}{\frac{1}{h_m} + \frac{1}{CRF \cdot 15170exp\left(-\frac{121620}{RT_s}\right)}} A_p C_t . \left(y_{H_2O} - \frac{y_{H_2} y_{CO}}{K_{1,eq}}\right)$	[20, 24]
R11	$CH_{0.65}O_{0.25} + CO_2 \rightarrow 2\ CO + 0.25\ H_2O + 0.075H_2$	$\frac{1}{\frac{1}{h_m} + \frac{1}{CRF \cdot 36.16\ exp\left(-\frac{77390}{RT_s}\right)}} A_p C_t . \left(y_{CO_2} - \frac{y_{CO}^2}{K_{2,eq}}\right)$	[20, 24]

2.4. Conservation equations

The mathematical formulation of the different physical and chemical phenomena involved in the three sub-processes of biomass gasification in the downdraft gasifier is given by the following set of conservation equations written in a macroscopic form and in two dimensional cylindrical coordinates:

2.4.1. Continuity equation

The continuity equation for the gas phase is given by:

$$\varepsilon\frac{\partial\langle\rho\rangle^f}{\partial t}+\frac{1}{r}\frac{\partial(\varepsilon r\langle\rho\rangle^f\langle U\rangle)}{\partial r}+\frac{\partial(\varepsilon\langle\rho\rangle^f\langle W\rangle)}{\partial z}=(1-\varepsilon)\left[k_{vap}\langle\rho_m\rangle^s+k_p\nu_V\langle\rho_b\rangle^s\right]+\sum_i\sum_j\varepsilon\,\nu_{ij}\overline{w}_i\langle r_j\rangle^f \quad (7)$$

Where the term on the right represents the source term describing the conversion of the solid biomass into gas. Specifically, it includes water vapor from moisture evaporation, volatile compounds from biomass pyrolysis and light gases from char oxidation and reduction.

2.4.2. Moisture conservation equation

$$(1-\varepsilon)\frac{\partial\langle\rho_m\rangle^s}{\partial t}+\frac{\partial(\langle\rho_m\rangle^s\langle W_b\rangle)}{\partial z}=-(1-\varepsilon)k_{vap}\langle\rho_m\rangle^s \quad (8)$$

Where W_b is the axial velocity of the solid biomass.

2.4.3. Solid phase conservation equations

The conservation equations for the solid phase, i.e. for the biomass and char respectively, are given by:

$$(1-\varepsilon)\frac{\partial\langle\rho_b\rangle^s}{\partial t}+\frac{\partial(\langle\rho_b\rangle^s\langle W_b\rangle)}{\partial z}=-(1-\varepsilon)k_p\langle\rho_b\rangle^s \quad (9)$$

$$(1-\varepsilon)\frac{\partial\langle\rho_c\rangle^s}{\partial t}+\frac{\partial\langle\rho_c\rangle^s\langle W_c\rangle}{\partial z}=(1-\varepsilon)\nu_c k_p\langle\rho_b\rangle^s-\left(\sum_i\sum_j\varepsilon\,\nu_{ij}\overline{w}_i\langle r_j\rangle^f\right) \quad (10)$$

Where W_c is the axial velocity of the char particles. While biomass is continuously consumed through pyrolysis, the source term of the char conservation equation includes a production positive term due to pyrolysis reaction and a consumption negative term due to char consumption by the heterogeneous oxidation and reduction reactions.

Besides, the biomass mass conservation equation (9) is used to calculate the variation of biomass density while keeping its velocity as constant. Conversely, the char mass conservation equation (10) is used to evaluate the local solid velocity while keeping the char density as constant.

2.4.4. Energy conservation equations

The local non thermal equilibrium which consists of the separate treatment of the energy equations for the solid and gas phases was also adopted in modeling of the heat transfer. Thus, the energy conservation equations for the fluid and solid phases involve convective and diffusive transfer mechanisms as well as the interfacial convective transfer and the source terms due to exothermic and endothermic reactions. The energy equations for the fluid and solid phases are respectively given by:

$$(1-\varepsilon)\frac{\partial\left(\langle\rho_s\rangle^s C_{p_s}\langle T_s\rangle^s\right)}{\partial t}+\langle\rho_s\rangle^s C_{p_s}\langle W_s\rangle\frac{\partial\langle T_s\rangle^s}{\partial z}=\frac{1}{r}\frac{\partial}{\partial r}\left(r(1-\varepsilon)\lambda_{s,eff}\frac{\partial\langle T_s\rangle^s}{\partial r}\right)$$
$$+\frac{\partial}{\partial z}\left((1-\varepsilon)\lambda_{s,eff}\frac{\partial\langle T_s\rangle^s}{\partial z}\right)+\sum_{j,het}(1-\varepsilon)\Delta H_j\langle r_j\rangle^s+h_{s-g}A_p\left(\langle T_g\rangle^f-\langle T_s\rangle^s\right) \quad (11)$$

$$\varepsilon\frac{\partial\left(\langle\rho\rangle^f C_{p_g}\langle T_g\rangle^f\right)}{\partial t}+\varepsilon\langle\rho\rangle^f\langle U\rangle C_p\frac{\partial\langle T_g\rangle^f}{\partial r}+\varepsilon\langle\rho\rangle^f\langle W\rangle C_p\frac{\partial\langle T_g\rangle^f}{\partial z}$$
$$=\frac{1}{r}\frac{\partial}{\partial r}\left(\varepsilon r\lambda_{g,eff}\frac{\partial\langle T_g\rangle^f}{\partial r}\right)+\frac{\partial}{\partial z}\left(\varepsilon\lambda_{g,eff}\frac{\partial\langle T_g\rangle^f}{\partial z}\right)+\sum_{j,hom}\varepsilon\Delta H_j\langle r_j\rangle^f-h_{s-g}A_p\left(\langle T_g\rangle^f-\langle T_s\rangle^f\right) \quad (12)$$

Where the effective gas thermal conductivity comprises conductive λ_g and dispersive λ_{dis} components [10]:

$$\lambda_{g,eff}=0.8\,\lambda_g+\lambda_{dis} \quad (13)$$

2.4.5. Gas species conservation equation

The gaseous species involved in the thermo-chemical conversion are transported through the voids of the packed bed. The conservation equation of a species *j* is expressed in term of its concentration and is given by:

$$\varepsilon\frac{\partial\langle C_j\rangle^f}{\partial t}+\varepsilon\langle U\rangle\frac{\partial\langle C_j\rangle^f}{\partial r}+\varepsilon\langle W\rangle\frac{\partial\langle C_j\rangle^f}{\partial z}=\frac{1}{r}\frac{\partial}{\partial r}\left(\varepsilon r D_{j,eff}\frac{\partial\langle C_j\rangle^f}{\partial r}\right)+\frac{\partial}{\partial z}\left(\varepsilon D_{j,eff}\frac{\partial\langle C_j\rangle^f}{\partial r}\right)+\varepsilon\langle R_i\rangle^f \quad (14)$$

Where the effective diffusivity is given by a molecular D_m and dispersive D_{dis} components [10]:

$$D_{i,ef} = 0.8\, D_m + D_{dis} \tag{15}$$

2.4.6. Momentum conservation equation

The momentum transport equation through the packed bed includes the Darcy and the Forchheimer drag terms. The momentum conservation equation in the radial and axial directions of the reactor is given by:

$$\varepsilon\frac{\partial(\rho\langle U\rangle)}{\partial t} + \varepsilon\rho\langle U\rangle\frac{\partial\langle U\rangle}{\partial r} + \varepsilon\rho\langle W\rangle\frac{\partial\langle U\rangle}{\partial z} = -\varepsilon\frac{\partial P}{\partial r} - \left(\varepsilon\frac{\mu}{\alpha}\langle U\rangle + \frac{\beta\rho(1-\varepsilon)}{d_p\varepsilon^3}\langle U\rangle^2\right) + \varepsilon\mu\left(\frac{\partial}{\partial r}\left(\frac{1}{r}\frac{\partial(r\langle U\rangle)}{\partial r}\right) + \frac{\partial^2\langle U\rangle}{\partial z^2}\right) \tag{16}$$

$$\varepsilon\frac{\partial(\rho\langle W\rangle)}{\partial t} + \varepsilon\rho\langle U\rangle\frac{\partial\langle W\rangle}{\partial r} + \varepsilon\rho\langle W\rangle\frac{\partial\langle W\rangle}{\partial z} = -\varepsilon\frac{\partial P}{\partial z} - \left(\varepsilon\frac{\mu}{\alpha}\langle W\rangle + \frac{\beta\rho(1-\varepsilon)}{d_p\varepsilon^3}\langle W\rangle^2\right) + \varepsilon\mu\left(\frac{1}{r}\frac{\partial}{\partial r}\left(r\frac{\partial\langle W\rangle}{\partial r}\right) + \frac{\partial^2\langle W\rangle}{\partial z^2}\right) \tag{17}$$

Where α and β are flow-resistance parameters.

2.5. Resolution method

The conservation equations constitute a set of non-linear coupled equations. The numerical resolution is therefore necessary. Firstly, the conversion of the non-linear equations into algebraic equations is performed using the finite volume method. The convective and diffusive terms of the transport equations are treated using the power law scheme. Then, the SIMPLE algorithm of Patankar [25] is used for the iterative resolution.

A FORTRAN code was established to perform the calculations. Convergence was monitored in terms of total residuals (10^{-4} for the energy conservation equations and 10^{-3} for the other equations).

3. Model validation

The numerical results of the developed model are compared with the experimental data obtained from running of our pilot downdraft gasifier. Indeed, an experimental investigation of almond shell gasification in a pilot downdraft gasifier was conducted by the authors in a previous paper [13]. The experimental data obtained are the temperature profiles along the axis of the reactor and the syngas composition at the outlet of the setup. The validation of the developed model is performed using the syngas composition. The molar composition of the syngas produced at the outlet of the reactor is numerically computed and presented in Table 4 along with the mean experimental fractions obtained by averaging the measured values from the gas analyzer. It could be seen that a satisfactory agreement is found for the main gases fractions (except methane) with an absolute average deviation of about 11%. The slight over prediction of carbon monoxide fraction could be explained by the high extent of the oxidation reactions. As a result, the predicted values of hydrogen and methane fractions are lower than the experimental values, which essentially yield carbon monoxide in the first step. Particularly, the high methane fraction found experimentally is probably caused by a high production of this species through the cracking and reforming of the tar species. The low methane fraction computed by the model indicates that the chemical mechanism does not cover the cracking reactions perfectly. Globally, the comparison of the model results with the experimental data shows that the syngas molar fractions are in reasonable agreement with the experimental data. Indeed, the chemical mechanism cannot account for all of the complex partial oxidation, thermal cracking and reforming reactions. Thus, the calculated syngas fractions could be considered acceptable and the model is validated against the experimental data.

Table 4. Comparison of syngas composition computed by the model with the experimental data

Species	CO	H_2	CH_4	CO_2	N_2
Experimental data	14.48	8.58	3.85	11.55	60.94
Calculated fractions	18.45	9.58	0.86	11.40	58.70

4. Simulation results

4.1. Distribution of the temperature fields in the three reactive zones of the reactor

The contour profiles of the solid and gas temperatures are given in Figure 3. The oxidation front is spread over the oxidation zone and the maximum char temperature reaches a value around 1440K. A similar trend is observed in the gas temperature distribution due to the continuous interaction through the convective heat transfer. The gas temperature reaches a higher level of about 1900K which could be explained by several reasons among which the high enthalpies of gas species and tar oxidation reactions and the low volumetric heat capacity of the gaseous phase compared to that of the solid phase. Indeed, volatile compounds usually react quickly in oxidative environment [8, 10, 11] while the char oxidation reaction is relatively slower because it can be limited

by external and internal diffusion of oxygen to the char surfaces. Both char and gas temperatures decrease smoothly in the reduction zone due to the endothermic gasification reactions. Moreover, the thermal equilibrium is progressively reached far from the oxidation front. Indeed, the endothermic gasification reactions take place in a fairly slower rate than the oxidation reactions. Thus, the magnitude of the interfacial heat transfer between the solid and gas phases becomes more important and the difference of temperature decays between the two phases in the reduction zone. However, the contour plots of the char and gas temperature show that the temperatures in the pyrolysis zone did not increase. The solid temperature distribution shows that the biomass pyrolysis occurs just in a thin layer close the oxidation front which can be explained by the limited heat transfer to the upper part of the reactor and the endothermic reactions (moisture evaporation and pyrolysis). This indicates also that heat transfer toward the upper biomass particles is made by local conduction. Thus, the temperature distribution can be improved in the pyrolysis zone by more adequate modeling of the radiation heat transfer from the oxidation front toward the top of the reactor where biomass pyrolysis and drying take place.

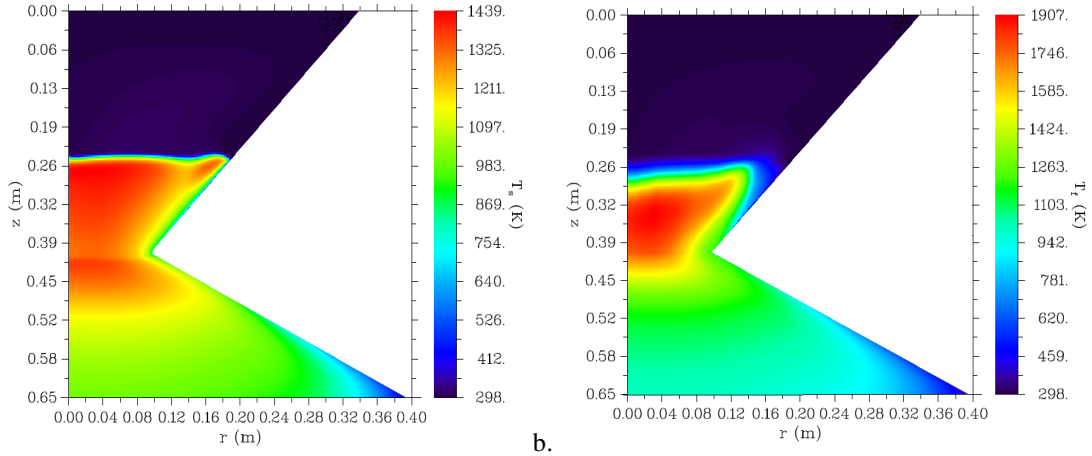

a. b.

Figure 3. Solid (a) and gas temperature (b) distributions in the three reactive zones of the downdraft gasifier

4.2. Distribution of the species concentrations

Carbon monoxide and hydrogen are the main desired gases in gasification. The contour profiles of these species are presented in Figure 4. Their concentrations increase progressively in the fixed bed gasifier. Firstly, in the pyrolysis zone, no clear distribution is observed because of the limited layer as observed in the previous simulations. Then, in the partial oxidation zone, carbon monoxide is intensively produced because it is the major product from the partial oxidation of the volatile gases and tar. It is also partially produced from the char oxidation reaction. Its concentration at the throat level and at the outlet of the reactor is far higher than that of hydrogen. On the other hand, hydrogen concentration is starting to increase in the partial oxidation zone and increases more importantly in the reduction zone due to the char gasification reactions, specifically the water gas reaction (R10). Moreover, the water gas shift reaction (R8) contributes considerably in the production of hydrogen in the reduction zone. Indeed, the activity of this reaction is promoted by the higher availability of carbon monoxide and the higher volume of the reduction domain compared to the partial oxidation domain.

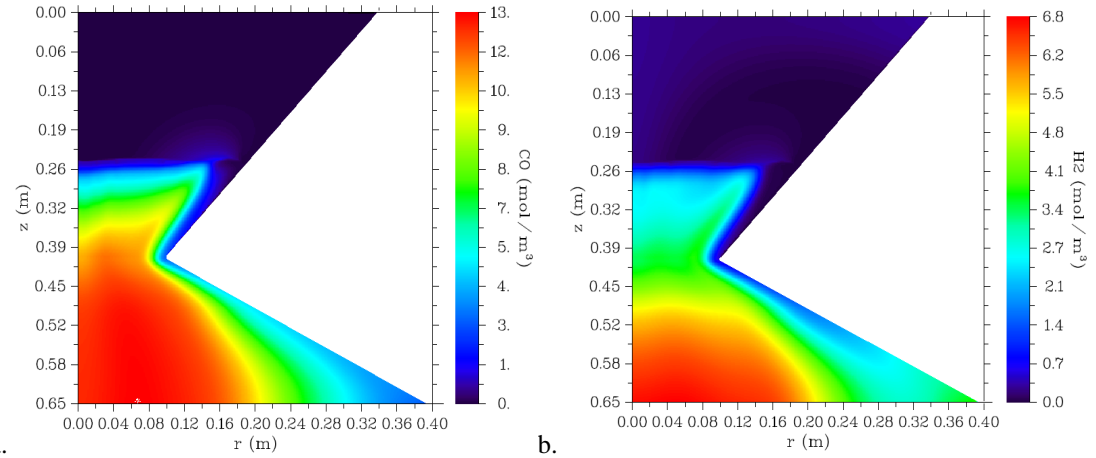

a. b.

Figure 4. Carbon monoxide (a) and hydrogen (b) concentrations profiles in the three reactive zones of the downdraft gasifier

5. Conclusion

In this study, a two dimensional model was presented for a pilot downdraft gasifier based on the conservation equations coupled with the heterogeneous and homogeneous chemical reactions. The model enabled the simulation of the temperature and concentration profiles inside the computational domain. The distributions highlighted the position of the oxidation front whereas the species distributions helped in the localization of the chemical reactions phenomena in both partial oxidation and reduction zone. However, particular attention should be paid to modeling the heat transfer mechanism toward the pyrolysis zone.

Références

[1] E. G. Pereira, J. N. Silva, J. L. Oliveira, C. S. Machado. Sustainable energy: A review of gasification technologies. Renewable and Sustainable Energy Reviews 16 (2012) 4753– 4762

[2] Key World Energy Statistics, Report of the International Energy Agency (IEA), 2014

[3] T. K. Patra, P. N. Sheth, Biomass gasification models for downdraft gasifier: A state-of the- art review, Renewable and Sustainable Energy Reviews 50 (2015) 583–593

[4] D. Baruah, D. C. Baruah, Modeling of biomass gasification: A review, Renewable and Sustainable Energy Reviews 39 (2014) 806–815

[5] C. Di Blasi, C. Branca, Modeling a stratified downdraft wood gasifier with primary and secondary air entry, Fuel 104 (2013) 847–860

[6] M. A. Masmoudi, K. Halouani, M. Sahraoui. Numerical modeling of combined partial oxidation and gasification zones in a downdraft gasifier fueled by almond shell. 5th International Renewable Energy Congress (IREC), Tunisia, 2014

[7] C. Mandl, I. Obernberger, F. Biedermann. Modelling of an updraft fixed-bed gasifier operated with softwood pellets. Fuel 2010; 89: 3795– 806

[8] H. Khodaei, Y. M. Al-Abdeli, F. Guzzomi, G. H. Yeoh. An overview of processes and considerations in the modeling of fixed-bed biomass combustion, Energy 2015; 88: 946 -972

[9] R. Johansson, H. Thunman, B. Leckner. Influence of intraparticle gradients in modeling of fixed bed combustion. Combust. Flame 2007; 149: 49–62

[10] S. Hermansson, H. Thunman. CFD modelling of bed shrinkage and channelling in fixed-bed combustion. Combust. Flame 2011; 158: 988–99

[11] J. Collazo, J. Porteiro, D. Patino, E. Granada. Numerical modeling of the combustion of densified wood under fixed-bed conditions. Fuel 2012; 93(1): 149–59

[12] R. Mehrabian, A. Shiehnejadhesar, R. Scharler, I. Obernberger. Multi-physics modelling of packed bed biomass combustion. Fuel 2014; 122: 164–78

[13] M. A. Masmoudi, M. Sahraoui, N. Grioui, K. Halouani, 2-D Modeling of thermo-kinetics coupled with heat and mass transfer in the reduction zone of a fixed bed downdraft biomass gasifier, Renewable Energy 66 (2014) 288- 298

[14] N. Grioui, K. Halouani, A. Zoulalian, F. Halouani. Thermochemical modeling of isothermal carbonization of thick wood particle – Effect of reactor temperature and wood particle size. Energy Conversion and Management 48 (2007) 927–936

[15] J. Shen, C. Igathinathane, M. Yu, A. K. Pothula, Biomass pyrolysis and combustion integral and differential reaction heats with temperatures using thermogravimetric analysis/differential scanning calorimetry, Bioresource Technology 185 (2015) 89–98

[16] K. P. Shadangi, K. Mohanty, Kinetic study and thermal analysis of the pyrolysis of non-edible oilseed powders by thermogravimetric and differential scanning calorimetric analysis, Renewable Energy 63 (2014) 337- 344

[17] X. Cao, J. Zhao, X. Wang, Y. Fan, X. Wei Zhao, Pyrolysis kinetics of soybean straw using thermogravimetric analysis. Fuel 169 (2016) 93-98

[18] Y. B. Yang, C. Ryu, A. Khor, N. E. Yates, V. N. Sharifi, J. Swithenbank. Effect of fuel properties on biomass combustion Part II Modeling approach— identification of the controlling factors. Fuel 84 (2005) 2116–2130

[19] J. C. Wurzenberger, S. Wallner, H. Raupenstrauch, J. G. Khinast. Thermal conversion of biomass: Comprehensive reactor and particle modeling, AIChE Journal 2002; 48: 2398- 411

[20] B.V. Babu, N.P. Sheth. Modeling and simulation of reduction zone of downdraft biomass gasifier: Effect of char reactivity factor, Energy Conversion and Management 47 (2006) 2602–2611.

[21] Y. Su, Y. Luo, Y. Chen, W. Wu, Y. Zhang. Experimental and numerical investigation of tar destruction under partial oxidation environment. Fuel Processing Technology 92 (2011) 1513–1524

[22] P. Bernada, F. Marias, A. Deydier, F. Couture, A. Fourcault, Modelling of a Traveling Bed waste Gasifier, Waste Biomass Valorization (2012) 3: 333–353

[23] R. Trane, S. Dahl, M.S. Skjøth-Rasmussen, A.D. Jensen, Catalytic steam reforming of bio-oil, International Journal of Hydrogen Energy 37 (2012) 6447 – 6472
[24] F. Weiland, H. Wiinikka, H. Hedman, J. Wennebro, E. Pettersson, R. Gebart. Influence of process parameters on the performance of an oxygen blown entrained flow biomass gasifier, Fuel 153 (2015) 510–519
[25] S. V. Patankar. Numerical heat transfer and fluid flow. NY: Hemisphere Publication, McGraw-Hill; 1980.